

**IDETC2019-97628**

**THERMOMECHANICAL TOPOLOGY OPTIMIZATION OF LATTICE HEAT TRANSFER  
STRUCTURE INCLUDING NATURAL CONVECTION AND DESIGN DEPENDENT  
HEAT SOURCE**

**Tong Wu**

Dept. of Mechanical Engineering  
Purdue University  
West Lafayette, Indiana, USA  
wu616@purdue.edu

**Joel C. Najmon**

Dept. of Mechanical Engineering  
Purdue University  
West Lafayette, Indiana, USA  
jnajmon@purdue.edu

**Andres Tovar**

Dept. of MechC and Energy Engr.  
Purdue School of Engr. and Technology  
IUPUI, Indianapolis, Indiana, USA  
tovara@iupui.edu

**ABSTRACT**

*Lattice Heat Transfer (LHT) structures provide superior structural support while improving the heat transfer coefficient through their high surface-to-volume ratios. By using current Additive Manufacturing (AM) technologies, LHT with highly complex structures is possible. In this study, the design concept of LHT is further improved by implementing a thermomechanical topology optimization method. With utilization of design-dependent heat source, the method can be applied to generate stiffer LHT structures under mechanical and thermomechanical loads, without decreasing their thermal performance; relative to a design made of a uniform LHT having the same mass fraction. Two numerical examples are presented to illustrate how to use the proposed approach to design LHT sections. The results show that the mechanical performance can be improved more than 50% compared to a uniform LHT with the same mass fraction, without decreasing the thermal performance. The method does not require a fluid mechanics model, thus it is computationally effective and particularly suitable for the conceptual design stage. The resulting optimized lattice is made possible by utilizing additive manufacturing technologies.*

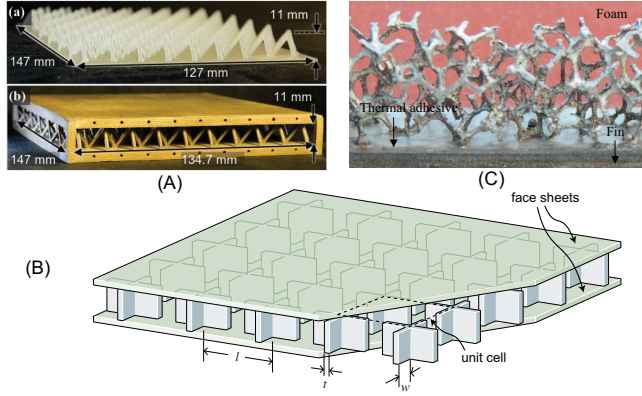
Keywords: Lattice heat transfer; thermomechanical; design-dependent heat source; topology optimization.

**1 Introduction**

Lattice Heat Transfer (LHT) structures provide superior structural support while improving the heat transfer coefficient through their high surface-to-volume ratios [1–3] (Fig. 1). The accelerated development of additive Manufacturing (AM/3D Printing) technologies enables the design and production of intricate lattice structures, offering significant cost savings, particularly in designs having high geometric complexity [4–6]. Recently, the multifunctional advantages of lattice structures has made them popular in applications which simultaneously require mechanical high strength and heat transfer rate [7,8], such as gas turbine blades and injection mold cooling systems. In gas turbine blades, inserting lattice structures as a cooling layer maintains sufficient structural blade strength, while improving the heat transfer rate two to three times compared to that of a smooth channel [9–11]. Lattice layers have been implemented as cooling system for injection molding, leading to a 20% reduction in cooling time, compared to the design having non-lattice conformal cooling [12–14]. Current LHT structures are mainly composed of uniformly distributed unit cells each having the same randomly generated foam-like porous medium, as well as structures similar to fins and pillar arrays (Fig. 1). A common way to find an optimized LHT structure is through analysis of simulation (recorded after designs are generated) and experimental data (recorded after the structures are produced) [1–3, 7, 8]. However, this approach limits design freedom, utilizing sample data methods that do not ensure optimality of the structure. To overcome

---

This is the author's manuscript of the article published in final edited form as:



Ref: (A) K N Son, et al., 2017; (B) D T Queheillalt et al., 2008; (C) SS Feng et al., 2014

**FIGURE 1.** MULTIFUNCTIONAL LATTICE HEAT SINK WITH (A) TETRAHEDRAL LATTICE [8] AND (B) TRUNCATED SQUARE [7], AND (C) METAL FOAM [1].

these drawbacks, in this study, a topology optimization approach is proposed to attain flexible and complex lattice structures that significantly improve the design optimality.

Since a LHT structure is required to transfer heat while withstanding mechanical and thermal stresses induced by the loads and the temperature gradient, a thermomechanical topology optimization should be incorporated to optimize a LHT structure. Traditional thermomechanical topology optimization has been employed to create thermal actuators [15–17], a thermal management device for spacecraft [18–20], and injection molds [21, 22]. However, in these approaches convective heat transfer on the structure’s boundary surfaces are not considered and remain scarce in literature. The thermomechanical topology optimization scheme employed in this study considers the convective heat transfer on these surfaces.

Convective heat transfer models that have been discussed in the context of topology optimization theory are primarily composed of a thermal-fluid (conjugate) heat transfer model, or a solid-structure heat transfer model. In thermal-fluid model based topology optimization, natural and forced convective heat transfer are affected by a fluid field resulting from Navier-Stokes equation or Darcy equation [23–25]. Consequently it can be time-consuming to couple with the thermomechanical model and unattractive for early stage conceptual design studies. An alternative approach is to employ a design-dependent heat source in the topology optimization of heat transfer problem without a fluid model. The design-dependent heat source varies with the element states or material itself. This was originally used to solve heat conduction topology optimization problems [26]. Further, design-dependent heat source implementation has been done to analyze heat transfer models that consider heat conduction, convection, and internal heat generation [27–29].

In this study, convective heat transfer and design-dependent

heat sources are coupled with a thermomechanical model, resulting in a novel topology optimization method. The method is specifically tailored to the design of multifunctional lattice heat transfer (LHT) structures requiring adequate thermal, mechanical and thermomechanical performance. In this method, it is assumed the design-dependent heat source is only located at the fluid phase, and the optimized fluid and solid phase distribution is available as a result of thermomechanical topology optimization. The paper is organized as follows: In section two, the finite element analysis of thermomechanical model is briefly presented. In section three, the proposed thermomechanical topology optimization including sensitivity analysis is illustrated; Two numerical examples are shown in section four. Finally, the summary of this work is presented in section five.

## 2 Finite element analysis of thermomechanical model

In a coupled thermomechanical model, the purely mechanical and thermomechanical loads caused by non-uniform temperature field should be considered. The overall thermal and mechanical performance is significantly influenced by the heat source distribution. In this study, it is assumed that the heat source is only applied to areas containing fluid. With the application of the proposed method, the optimized shape, location and numbers of areas are obtained. Before the illustration of the method, procedures of thermomechanical finite element analysis (FEA) is briefly described as follows, where natural convection and design-dependent heat source are incorporated.

### 2.1 Thermal model with convection and design-dependent heat load

In a thermal model, the energy dissipation can be written as

$$Q = \frac{1}{2} \int_{\Omega} \nabla T^T \kappa(\theta) \nabla T d\Omega - W_q, \quad (1)$$

where  $\kappa$  is the thermal conductivity tensor,  $\nabla T$  indicates temperature gradients, and  $W$  is the external work. Discretizing Eq. (1) yields

$$Q = \frac{1}{2} \mathbf{T}(\theta)^T \mathbf{K}_t(\theta) \mathbf{T}(\theta) - \mathbf{q}^T \mathbf{T}(\theta), \quad (2)$$

In a static equilibrium state  $\frac{\partial Q}{\partial \mathbf{T}} = \mathbf{0}$ , the Fourier equation in Matrix form is formulated:

$$\mathbf{K}_t(\theta) \mathbf{T}(\theta) = \mathbf{q}(\theta) \quad (3)$$

where the global stiffness of heat transfer  $\mathbf{K}_t$  is composed of stiffness matrix of thermal conduction  $\mathbf{K}_{\text{cond}}$  and natural convection

$\mathbf{K}_{\text{conv}}$ :

$$\mathbf{K}_t(\boldsymbol{\theta}) = \mathbf{K}_{\text{cond}}(\boldsymbol{\theta}) + \mathbf{K}_{\text{conv}}(\boldsymbol{\theta}). \quad (4)$$

In Eq. (4),

$$\mathbf{K}_{\text{cond}}(\boldsymbol{\theta}) = \sum_{e=1}^{n_e} \int_{\Omega} \nabla \mathbf{N}^T \boldsymbol{\kappa}(\boldsymbol{\theta}) \nabla \mathbf{N} dV, \quad (5)$$

where

$$\boldsymbol{\kappa}(\boldsymbol{\theta}) = \boldsymbol{\kappa}_{\min} + (\boldsymbol{\kappa}_s - \boldsymbol{\kappa}_{\min}) \boldsymbol{\theta}^{p_1}, \quad (6)$$

where  $p_1$  is a penalty number. This material interpolation scheme indicates the thermal conductivity is higher when the solid material containing more volume in an element. Notably,  $\boldsymbol{\kappa}_{\min}$  is the minimum thermal conductivity for an element to avoid singularity in matrix computation. The stiffness of natural convection is formulated as

$$\mathbf{K}_{\text{conv}} = \sum_{e=1}^{n_e} h \int_S \mathbf{N}^T \mathbf{N} dS, \quad (7)$$

where  $h$  is convective heat transfer coefficient. In Eq. (3),  $\mathbf{q}$  is the boundary heat source vector which composed of constant heat source  $\mathbf{q}_0$  and a design-dependent heat source  $\mathbf{q}_0(\boldsymbol{\theta})$ .

$$\mathbf{q}(\boldsymbol{\theta}) = \mathbf{q}_0 + \mathbf{q}_0(\boldsymbol{\theta}), \quad (8)$$

where

$$\mathbf{q}_0(\boldsymbol{\theta}) = \sum_{e=1}^{n_e} h_1(\boldsymbol{\theta}) \int_S \mathbf{N} dS. \quad (9)$$

The design-dependency is represented by the following material interpolation function

$$h_1(\boldsymbol{\theta}) = h_f (1 - \boldsymbol{\theta}^{p_2}). \quad (10)$$

The design-dependent heat source is implemented through voids containing variable fluid levels. This material interpolation scheme assumes there is a maximum design-dependent heat source  $h_f$  when the element  $V$  is filled with fluid, and zero when the element is filled with solid. When the element is filled with fluid, the design dependent heat source  $\mathbf{q}_0$  reaches its maximum value  $\overline{\mathbf{q}_0}$ .

## 2.2 Thermomechanical model with convection and design-dependent heat load

Solving the heat transfer model will result in a non-uniform temperature field, which induces thermo-elastic strain and stress fields. For a thermomechanical structure, the strain and stress relations can be described by

$$\mathbf{D}(\boldsymbol{\varepsilon} - \boldsymbol{\varepsilon}_T) = \boldsymbol{\sigma} \quad (11)$$

where  $\mathbf{D}$  is the elasticity tensor, and  $\boldsymbol{\varepsilon}$  is strain due to mechanical load.  $\boldsymbol{\varepsilon}_T$  is strain due to thermal-elastic load coupling the temperature field derived from thermal model. The elementwise thermal-elastic strain  $\boldsymbol{\varepsilon}_T$  is formulated as

$$\boldsymbol{\varepsilon}_{Te} = \alpha(\boldsymbol{\theta}) (\mathbf{N} \mathbf{T}_e(\boldsymbol{\theta}) - T_0) \mathbf{1} \quad (12)$$

where  $\alpha$  is thermal expansion coefficient related to proportion of solid phase in the an element  $\boldsymbol{\theta}$  and penalty number  $p_3$ :

$$\alpha(\boldsymbol{\theta}) = \alpha_{\min} + (\alpha_0 - \alpha_{\min}) \boldsymbol{\theta}^{p_3}. \quad (13)$$

$\mathbf{T}_e(\boldsymbol{\theta})$  is the elemental temperature obtained from thermal model. The strain energy density is

$$\Phi = \frac{1}{2} \int_{\Omega} (\boldsymbol{\varepsilon} - \boldsymbol{\varepsilon}_T)^T \mathbf{D}(\boldsymbol{\theta}) (\boldsymbol{\varepsilon} - \boldsymbol{\varepsilon}_T) d\Omega - W, \quad (14)$$

Discretizing Eq. (14) yields

$$\Phi = \frac{1}{2} \mathbf{u}^T \mathbf{K}_{\text{elast}}(\boldsymbol{\theta}) \mathbf{u} - \mathbf{f}_{th}^T(\boldsymbol{\theta}, \mathbf{T}(\boldsymbol{\theta})) \mathbf{u} - \mathbf{f}^T \mathbf{u}, \quad (15)$$

In Eq. (15), the thermo-elastic load  $\mathbf{f}_{th}$  is given by

$$\mathbf{f}_{th}(\boldsymbol{\theta}, \mathbf{T}(\boldsymbol{\theta})) = \mathbf{K}_{mt}(\boldsymbol{\theta}) \mathbf{T}(\boldsymbol{\theta}), \quad (16)$$

where  $\mathbf{K}_{mt}$  is thermo-mechanical coupling stiffness matrix

$$\mathbf{K}_{mt}(\boldsymbol{\theta}) = \sum_{e=1}^{n_e} \int_V \mathbf{B}^T \mathbf{D}(\boldsymbol{\theta}_e) \alpha \mathbf{N} dV, \quad (17)$$

and node temperature  $\mathbf{T}(\boldsymbol{\theta})$  is derived from Eq. (15) associated to the thermal model.  $\mathbf{B}$  is the matrix representing strain-displacement relation. The stiffness matrix of elasticity,  $\mathbf{K}_{\text{elast}}$ , is

$$\mathbf{K}_{\text{elast}}(\boldsymbol{\theta}) = \sum_{e=1}^{n_e} \int_V \mathbf{B}^T \mathbf{D}(\boldsymbol{\theta}_e) \mathbf{B} dV. \quad (18)$$

where  $\mathbf{u}$  is the nodal displacement, and  $\mathbf{f}$  is the external force.

In a static equilibrium state  $\frac{\partial \Phi}{\partial \mathbf{u}} = \mathbf{0}$ , Hook's law in matrix form is formulated as

$$\mathbf{K}_{\text{elast}}(\boldsymbol{\theta})\mathbf{u}(\boldsymbol{\theta}) = \left( \mathbf{f}_{\text{th}}(\boldsymbol{\theta}, \mathbf{T}(\boldsymbol{\theta})) + \mathbf{f} \right)^{\text{T}} \quad (19)$$

### 3 Proposed thermomechanical topology optimization

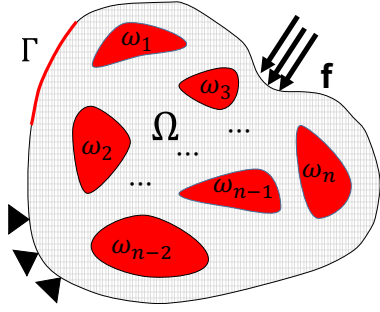


**FIGURE 2.** An Illustration of design domain, constant and design-dependent heat source for proposed method.

As aforementioned, the heat source can be divided to constant heat source  $\mathbf{q}_0$  and design-dependent heat source  $\mathbf{q}_0^i(\boldsymbol{\theta})$ . In this problem, we assume a constant heat source is applied to the boundary surface  $\Gamma$  in Figure. 2. As described in Eq. (9) and Eq. (10), the heat source is applied to the cavities  $\omega_1, \omega_2, \dots, \omega_n$  in Figure 2. The shape, location, area, and numbers of these cavities are unknown. These will be defined later with the proposed algorithm. However, the sum of these design-dependent heat sources should have an upper bound  $\bar{q}$ , if the volume fraction of all the cavities have an upper bound. These heat source conditions can be formulated as:

$$\begin{aligned} \mathbf{q}_0 &\in \Gamma, \quad \mathbf{q}_0^i(\boldsymbol{\theta}) \in \omega_i \quad (i = 1 \dots n), \\ \sum_{i=1}^n \mathbf{q}_0^i &= \bar{q} \end{aligned} \quad (20)$$

The heat load could induce a non-uniform temperature field, thus a thermal load field  $\mathbf{f}_{\text{th}}(\boldsymbol{\theta}, \mathbf{T}(\boldsymbol{\theta}))$  is obtained. A superposition of the internal thermal load and external mechanical load  $\mathbf{f}$  is applied as the total load to formulate the load of the thermomechanical problem.

In a thermomechanical topology optimization problem, it is desirable to obtain high thermal and mechanical performance. A common metric for thermal performance is heat compliance given by

$$J_t = \mathbf{q}(\boldsymbol{\theta})^{\text{T}} \mathbf{T}(\boldsymbol{\theta}). \quad (21)$$

For mechanical performance, the mechanical compliance is adopted as

$$J_m = \left( \mathbf{f}_{\text{th}}(\boldsymbol{\theta}, \mathbf{T}(\boldsymbol{\theta})) + \mathbf{f} \right)^{\text{T}} \mathbf{u}(\boldsymbol{\theta}). \quad (22)$$

In this study, mechanical compliance is used as the objective function for thermomechanical topology optimization. The thermal compliance is defined as a constraint that should be smaller than the reference value of the initial design,  $J_t^0$ :

$$\begin{aligned} \text{minimize} \quad & J_m(\boldsymbol{\theta}) \\ \text{subject to} \quad & J_t(\boldsymbol{\theta}) \leq J_t^0(\boldsymbol{\theta}) \end{aligned} \quad (23)$$

At the same time, the mass constraints for the structure and elements are given by

$$\begin{aligned} m(\boldsymbol{\theta}) &\leq m(\boldsymbol{\theta}_0) \\ \boldsymbol{\theta}^{\text{min}} &\leq \boldsymbol{\theta} \leq \boldsymbol{\theta}^{\text{solid}}, \end{aligned} \quad (24)$$

where  $m$  is the mass of the structure,  $m(\boldsymbol{\theta})_0$  is a given constant,  $\boldsymbol{\theta}^{\text{min}}$  is the minimum allowable density for each element (which is the relative density of fluid phase in this study), and  $\boldsymbol{\theta}^{\text{solid}}$  is the relative density of solid phase, equal to 1. Fourier's law Eq. (3) and Hook's law Eq. (19) must also be satisfied. Finally, the problem statement of the proposed thermomechanical topology optimization is

$$\begin{aligned} \text{find} \quad & \boldsymbol{\theta}^* \in \mathbb{R}^{n_c} \\ \text{minimize} \quad & J_m(\boldsymbol{\theta}) \\ \text{subject to} \quad & J_t(\boldsymbol{\theta}) \leq J_t^0(\boldsymbol{\theta}) \\ & m(\boldsymbol{\theta}) \leq m(\boldsymbol{\theta}_0) \\ & \boldsymbol{\theta}^{\text{min}} \leq \boldsymbol{\theta} \leq \boldsymbol{\theta}^{\text{solid}} \\ & \mathbf{q}_0 \in \Gamma, \quad \mathbf{q}_0^i(\boldsymbol{\theta}) \in \omega_i \quad (i = 1 \dots n), \\ & \sum_{i=1}^n \mathbf{q}_0^i = \bar{q} \\ \text{satisfying} \quad & \mathbf{q}(\boldsymbol{\theta}) = \mathbf{K}_t(\boldsymbol{\theta})\mathbf{T}(\boldsymbol{\theta}) \\ & \mathbf{f}_{\text{th}}(\boldsymbol{\theta}, \mathbf{T}(\boldsymbol{\theta})) + \mathbf{f} = \mathbf{K}_{\text{elast}}(\boldsymbol{\theta})\mathbf{u}(\boldsymbol{\theta}). \end{aligned} \quad (25)$$

### 3.1 Sensitivity analysis

To analyze the sensitivity of this problem Eq. (25) can be rewritten in the form of Lagrangian function  $\mathcal{L}$ :

$$\begin{aligned} \mathcal{L} = & \left( \mathbf{f}_{\text{th}}(\boldsymbol{\theta}, \mathbf{T}(\boldsymbol{\theta})) + \mathbf{f} \right)^\top \mathbf{u}(\boldsymbol{\theta}) + \lambda_J \left( \mathbf{q}(\boldsymbol{\theta})^\top \mathbf{T}(\boldsymbol{\theta}) - \beta J_t^0(\boldsymbol{\theta}) \right) + \\ & \boldsymbol{\lambda}_m^\top \left( \mathbf{K}_{\text{elast}}(\boldsymbol{\theta}) \mathbf{u}(\boldsymbol{\theta}) - \mathbf{f} - \mathbf{f}_{\text{th}}(\boldsymbol{\theta}, \mathbf{T}(\boldsymbol{\theta})) \right) + \\ & \boldsymbol{\lambda}_t^\top \left( \mathbf{K}_t(\boldsymbol{\theta}) \mathbf{T}(\boldsymbol{\theta}) - \mathbf{q}(\boldsymbol{\theta}) \right) \end{aligned} \quad (26)$$

Where  $\boldsymbol{\lambda}_m^\top$  and  $\boldsymbol{\lambda}_t^\top$  are adjoint vectors, and  $\lambda_J$  is a penalty which is activated when the thermal compliance is greater than the initial design value,  $\beta$  is a relaxation factor equal to 1.1:

$$\begin{aligned} \text{if } J_t(\boldsymbol{\theta}) \leq \beta J_t^0(\boldsymbol{\theta}), \quad \lambda_J = 0 \\ \text{otherwise } \quad \lambda_J = 1 \end{aligned} \quad (27)$$

Since  $\mathbf{f}_{\text{th}}$  a function of relative density  $\boldsymbol{\theta}$  and temperature  $\mathbf{T}(\boldsymbol{\theta})$ ,  $\mathbf{T}(\boldsymbol{\theta})$  is a function of  $\boldsymbol{\theta}$ , and  $\mathbf{q}(\boldsymbol{\theta})$  is a function of  $\boldsymbol{\theta}$ , the derivatives of the Lagrangian for each element  $\boldsymbol{\theta}$  are written as

$$\begin{aligned} \frac{\partial \mathcal{L}(\boldsymbol{\theta})}{\partial \boldsymbol{\theta}} = & \mathbf{u}(\boldsymbol{\theta})^\top \frac{\partial \mathbf{f}_{\text{th}}}{\partial \boldsymbol{\theta}} + \mathbf{u}(\boldsymbol{\theta})^\top \frac{\partial \mathbf{f}_{\text{th}}}{\partial \mathbf{T}(\boldsymbol{\theta})} \frac{\partial \mathbf{T}(\boldsymbol{\theta})}{\partial \boldsymbol{\theta}} + (\mathbf{f} + \mathbf{f}_{\text{th}})^\top \frac{\partial \mathbf{u}(\boldsymbol{\theta})}{\partial \boldsymbol{\theta}} + \\ & \lambda_J \mathbf{T}(\boldsymbol{\theta})^\top \frac{\partial \mathbf{q}(\boldsymbol{\theta})}{\partial \boldsymbol{\theta}} + \lambda_J \mathbf{q}^\top(\boldsymbol{\theta}) \frac{\partial \mathbf{T}(\boldsymbol{\theta})}{\partial \boldsymbol{\theta}} + \\ & \boldsymbol{\lambda}_m^\top \left( \frac{\partial \mathbf{K}_{\text{elast}}(\boldsymbol{\theta})}{\partial \boldsymbol{\theta}} \mathbf{u}(\boldsymbol{\theta}) + \mathbf{K}_{\text{elast}}(\boldsymbol{\theta}) \frac{\partial \mathbf{u}(\boldsymbol{\theta})}{\partial \boldsymbol{\theta}} \right. \\ & \left. - \frac{\partial \mathbf{f}_{\text{th}}}{\partial \boldsymbol{\theta}} - \frac{\partial \mathbf{f}_{\text{th}}}{\partial \mathbf{T}(\boldsymbol{\theta})} \frac{\partial \mathbf{T}(\boldsymbol{\theta})}{\partial \boldsymbol{\theta}} \right) + \\ & \boldsymbol{\lambda}_t^\top \left( \frac{\partial \mathbf{K}_t(\boldsymbol{\theta})}{\partial \boldsymbol{\theta}} \mathbf{T}(\boldsymbol{\theta}) + \mathbf{K}_t \frac{\partial \mathbf{T}(\boldsymbol{\theta})}{\partial \boldsymbol{\theta}} - \frac{\partial \mathbf{q}(\boldsymbol{\theta})}{\partial \boldsymbol{\theta}} \right) \end{aligned} \quad (28)$$

In order to cancel  $\frac{\partial \mathbf{u}(\boldsymbol{\theta})}{\partial \boldsymbol{\theta}}$  term and  $\frac{\partial \mathbf{T}(\boldsymbol{\theta})}{\partial \boldsymbol{\theta}}$ , the value in adjoint vectors can be defined to satisfy

$$\begin{aligned} ((\mathbf{f} + \mathbf{f}_{\text{th}})^\top + \boldsymbol{\lambda}_m^\top \mathbf{K}_{\text{elast}}(\boldsymbol{\theta})) \frac{\partial \mathbf{u}(\boldsymbol{\theta})}{\partial \boldsymbol{\theta}} = \mathbf{0} \\ \left( \mathbf{u}(\boldsymbol{\theta})^\top \frac{\partial \mathbf{f}_{\text{th}}}{\partial \mathbf{T}(\boldsymbol{\theta})} + \boldsymbol{\lambda}_t^\top \mathbf{K}_t(\boldsymbol{\theta}) \right. \\ \left. - \boldsymbol{\lambda}_m^\top \frac{\partial \mathbf{f}_{\text{th}}}{\partial \mathbf{T}(\boldsymbol{\theta})} + \lambda_J \mathbf{q}^\top(\boldsymbol{\theta}) \right) \frac{\partial \mathbf{T}(\boldsymbol{\theta})}{\partial \boldsymbol{\theta}} = \mathbf{0}, \end{aligned} \quad (29)$$

By sequentially solving the above two equations, the sensitivity

is derived as

$$\begin{aligned} \frac{\partial L(\boldsymbol{\theta})}{\partial \theta_c} = & \mathbf{u}(\boldsymbol{\theta})^\top \frac{\partial \mathbf{f}_{\text{th}}}{\partial \boldsymbol{\theta}} + \lambda_J \mathbf{T}(\boldsymbol{\theta})^\top \frac{\partial \mathbf{q}(\boldsymbol{\theta})}{\partial \boldsymbol{\theta}} + \\ & \boldsymbol{\lambda}_m^\top \left( \frac{\partial \mathbf{K}_{\text{elast}}(\boldsymbol{\theta})}{\partial \boldsymbol{\theta}} \mathbf{u}(\boldsymbol{\theta}) - \frac{\partial \mathbf{f}_{\text{th}}}{\partial \boldsymbol{\theta}} \right) \\ & + \boldsymbol{\lambda}_t^\top \left( \frac{\partial \mathbf{K}_t(\boldsymbol{\theta})}{\partial \boldsymbol{\theta}} \mathbf{T}(\boldsymbol{\theta}) - \frac{\partial \mathbf{q}(\boldsymbol{\theta})}{\partial \boldsymbol{\theta}} \right). \end{aligned} \quad (30)$$

### 4 Numerical examples

Two numerical examples are shown in this section, namely Design 1 and Design 2. Both of these two designs share the same boundary conditions associated to heat transfer, but their boundary condition for thermomechanical models are different. In Design 1, the bottom edge is fixed, and compressive pressure is imposed on the top edge. In Design 2, the boundary condition and mechanical load locations are following a typical Messerschmitt-Blkow-Blohm (MBB) beam example. Assume the initial design domain is composed of an X-bracing lattice structure having a mass fraction of  $m(\boldsymbol{\theta}_0)=0.5$ . The X-bracing lattice structure is adopted since it can be produced without requiring additional materials for supporting structure in additive manufacturing.

To reveal the capability of the proposed method, for each design, four scenarios (A-D) are examined. The results of the initial design for each four scenarios are listed as Scenarios *a-d*. In Scenario A and *a*, only thermal boundary conditions and supports for thermomechanical model are applied. All the mechanical loads are induced from a non-uniform temperature field derived from the heat transfer model. In Scenario B and *b*, an additional external constant heat flux is applied. Then, in Scenario C and *c*, an external pressure or force is imposed on the boundary. Finally, in Scenario D and *d*, the convective heat transfer coefficient is doubled. The penalization numbers values are  $p_1=5$ ,  $p_2=3$ , and  $p_3=1.2$ . The relative density of fluid phase  $\theta^{\text{min}}$  is equal to 0.15. For all of these examples, non-dimensional parameters are used.

#### 4.1 Example 1:A LHT section withstanding compressive mechanical load

In the first example, a rectangular design domain having  $120 \times 240$  elements is fixed at the bottom edge. In the thermal model, the design-dependent heat source is imposed on the entire design domain. The maximum value of the heat source value per element  $\bar{q}_0$  is 0.01, convective heat transfer coefficient  $h$  is equal to 0.005. The thermal model results in a non-uniform temperature field, inducing thermomechanical loads. In scenarios A and *a*, only the induced thermomechanical loads are considered in the mechanical model (Fig. 3). In scenarios B and *b*, a boundary heat source  $q_2=0.1$  is applied to each node on the bottom edge (Fig. 4). Then, in scenarios C and *c*, a compressive pressure

**TABLE 1.** A SUMMARY OF BOUNDARY CONDITION FOR SCENARIOS.

Scenario	1. Boundary condition of thermal problem	2. Boundary condition of thermomechanical problem
<i>a</i> and A	Volumetric design-dependent heat source	Thermomechanical load
<i>b</i> and B	In addition to volumetric design-dependent heat source, apply a constant heat source to the bottom edge	Thermomechanical load
<i>c</i> and C	In addition to volumetric design-dependent heat source, apply a constant heat source to the bottom edge	In addition to thermomechanical load, apply external mechanical load to the boundary edges
<i>d</i> and D	In addition to volumetric design-dependent heat source, apply a constant heat source to the bottom edge, increasing convective heat transfer coefficient	In addition to thermomechanical load, apply external mechanical load to the boundary edges

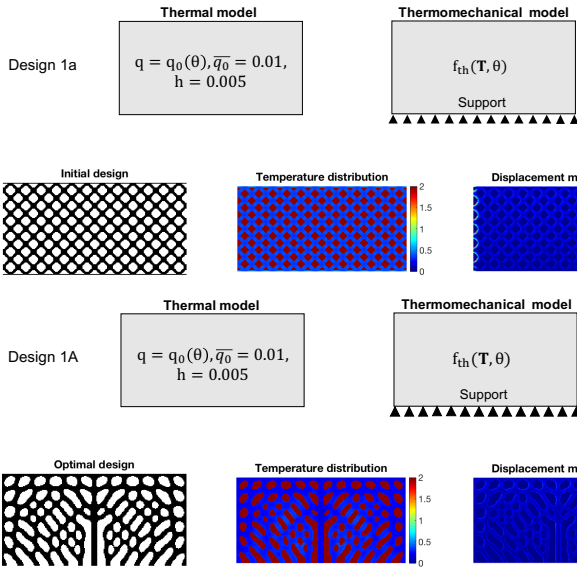


**FIGURE 3.** TOPOLOGY, TEMPERATURE DISTRIBUTION, AND DISPLACEMENT MAGNITUDE DISTRIBUTION OF INITIAL AND OPTIMAL DESIGN FOR SCENARIO 1a AND 1A.

$p=0.005$  is applied to each node on the top edge of the design domain (Fig. 5). In scenarios D and *d*, the convective heat transfer  $h$  is doubled from 0.005 to 0.01 (Fig. 6).

The topology, temperature distribution and displacement magnitude plot of the first example are shown in Fig. 3 to Fig. 6, and the key results are listed in Table 2. The mechanical compliance of optimal designs are only 40% to 52% of the initial designs, while thermal compliance is kept at 95% to 102% of the initial designs. Additionally, other metrics can also be compared such as mean displacement magnitude  $\| \widehat{u} \|$ , maximum displacement magnitude  $\| u \|$ , maximum temperature  $\widehat{T}$  and mean tem-

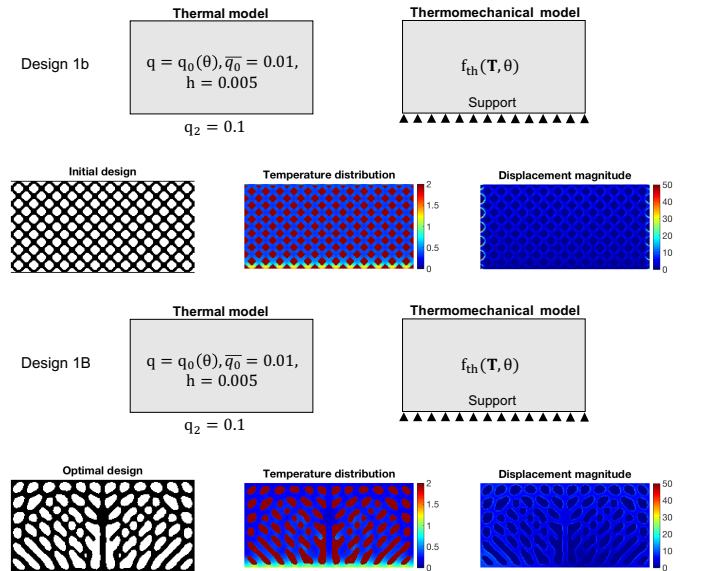


**FIGURE 4.** TOPOLOGY, TEMPERATURE DISTRIBUTION, AND DISPLACEMENT MAGNITUDE DISTRIBUTION OF INITIAL AND OPTIMAL DESIGN FOR SCENARIO 1b AND 1B.

perature  $\bar{T}$ . The magnitude of mean displacement of the optimal designs is 56% to 77% of the initial designs, and the maximum displacement of the optimal designs is only 21% to 27% of the initial designs. The mean temperature of the optimal designs is 91% to 94% of initial designs, which implies a limited compromising of thermal performance to achieve an increased mechanical performance. The maximum temperature of the optimal designs is 72% to 102% of the initial designs, which implies that the overall heat transfer performance is generally maintained, but that the local heat transfer performance is not be guaranteed.

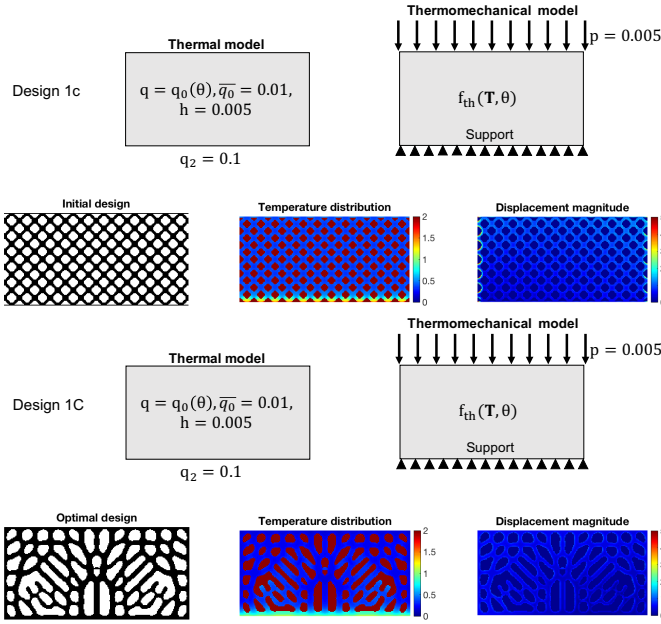


**FIGURE 5.** TOPOLOGY, TEMPERATURE DISTRIBUTION, AND DISPLACEMENT MAGNITUDE DISTRIBUTION OF INITIAL AND OPTIMAL DESIGN FOR SCENARIO 1c AND 1c.

**TABLE 2.** KEY RESULTS OF EXAMPLE 1: A LHT SECTION WITHSTANDING COMPRESSIVE MECHANICAL LOAD.

Case	$J_m(\theta)$	$J_t(\theta)$	$\ \widehat{u}\ $	$\ \overline{u}\ $	$\widehat{T}$	$\overline{T}$
Design 1a	285.90	1843.1	2.3133	47.617	0.9331	2.1032
Design 1A	160.38	1736.4	1.7944	10.006	0.9027	2.1518
Design 1b	282.53	1863.1	2.3755	47.718	1.0408	2.7952
Design 1B	152.36	1758.1	1.8206	10.172	0.9477	2.153
Design 1c	301.76	1863.1	4.2062	50.115	1.0408	2.7952
Design 1C	158.8	1798.4	2.672	11.392	0.9571	2.164
Design 1d	83.613	958.25	3.1024	27.8121	0.5212	1.8108
Design 1D	33.704	984.42	1.7487	7.5790	0.4945	1.3121

#### 4.2 Example 2: A LHT section with boundary conditions of a MBB beam

In the second example, the thermal model remains the same as the first example with the exception that the supports are located at left edge and the right bottom corner, in terms of a half MBB beam. In scenarios A and a, only the induced thermomechanical loads are considered in the mechanical model (Fig. 7). In scenarios B and b, a boundary heat source  $q_2=0.1$  is applied to each node on the bottom edge (Fig. 8). Then, in scenarios C and c, an external load  $p=1.2$  is applied to the top left corner of the design domain (Fig. 9). In scenarios D and d, the convective

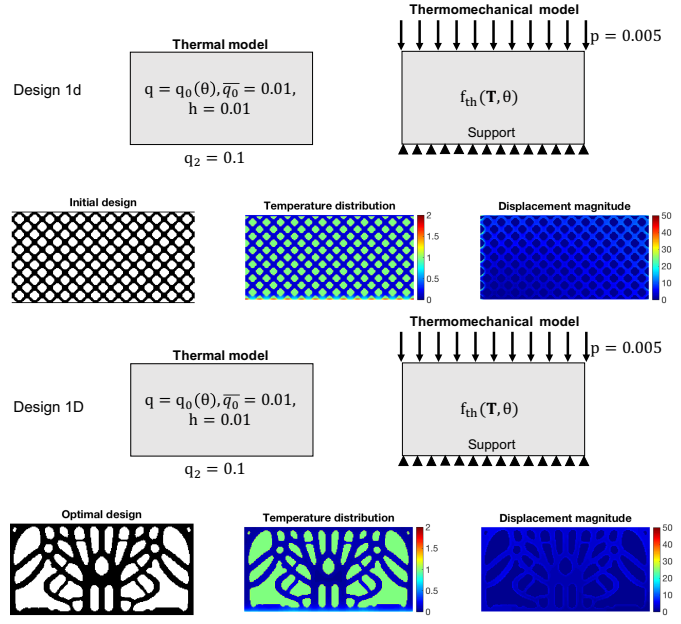


**FIGURE 6.** TOPOLOGY, TEMPERATURE DISTRIBUTION, AND DISPLACEMENT MAGNITUDE DISTRIBUTION OF INITIAL AND OPTIMAL DESIGN FOR SCENARIO 1d AND 1D.

heat transfer  $h$  is doubled from 0.005 to 0.01 (Fig. 10).

The topology, temperature distribution and displacement magnitude plot of the second example are shown in Fig. 3 to Fig. 6, and the key results are listed in Table 3. The results show trends similar to the first example: The mechanical compliance of optimal designs is only 27% to 46% of the initial designs, while thermal compliance is maintained at 94% to 110% of the initial designs. The magnitude of mean displacement of the optimal designs is 26% to 79% of the initial designs, and the maximum displacement of the optimal designs is only 22% to 46% of the initial designs. The mean temperature of the optimal designs is 91% to 100% of initial designs, which again implies a limited compromising of thermal performance to achieve an increased mechanical performance. The maximum temperature of the optimal designs is 73% to 103% of the initial designs, which implies that the overall heat transfer performance is generally maintained, but that the local heat transfer performance is not guaranteed.

## 5 Conclusion

This study presents a novel thermomechanical topology optimization method with consideration of convective heat transfer and design-dependent heat sources, that takes advantage of the benefits of a multifunctional LHT structure. The heat source is dependent on the material phase, thus the optimized solid-fluid interface and heat source distribution can be obtained through

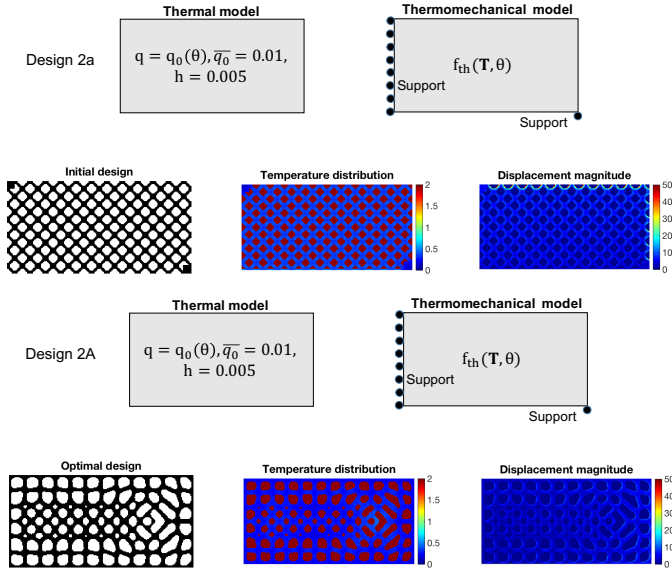


**FIGURE 7.** TOPOLOGY, TEMPERATURE DISTRIBUTION, AND DISPLACEMENT MAGNITUDE DISTRIBUTION OF INITIAL AND OPTIMAL DESIGN FOR SCENARIO 2a AND 2A.

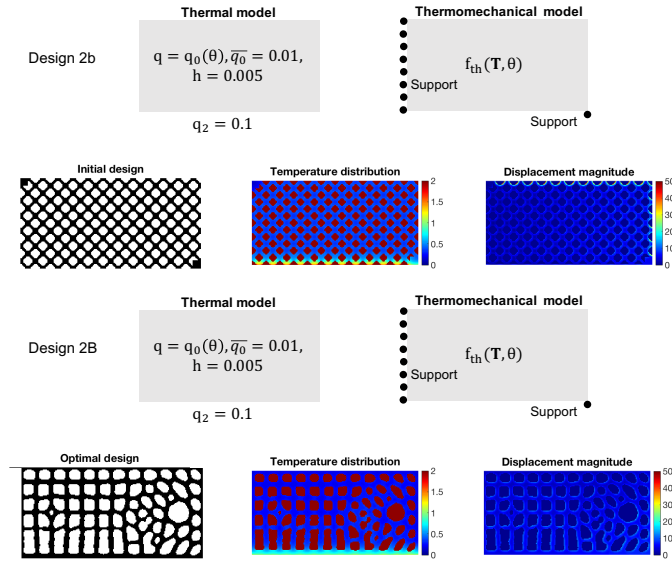


**FIGURE 8.** TOPOLOGY, TEMPERATURE DISTRIBUTION, AND DISPLACEMENT MAGNITUDE DISTRIBUTION OF INITIAL AND OPTIMAL DESIGN FOR SCENARIO 2b AND 2B.

the method. Since the method does not require a fluid mechanics model, it is computationally efficient and convenient for application in the conceptual design stage. With the application of this method, the mechanical stiffness of the LHT structure due to mechanical and thermomechanical loads is significantly improved,

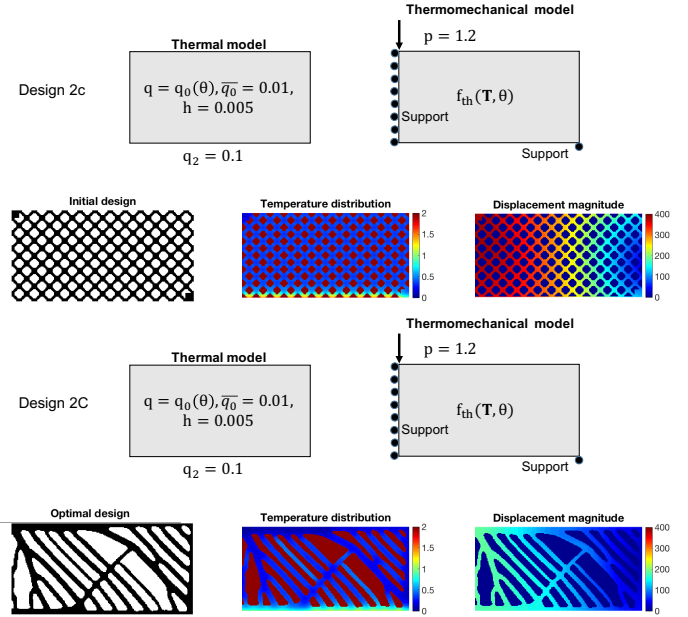


**FIGURE 9.** TOPOLOGY, TEMPERATURE DISTRIBUTION, AND DISPLACEMENT MAGNITUDE DISTRIBUTION OF INITIAL AND OPTIMAL DESIGN FOR SCENARIO 2c AND 2C.

**TABLE 3.** KEY RESULTS OF EXAMPLE 2: A LHT SECTION WITH BOUNDARY CONDITIONS OF A MBB BEAM.

Case	$J_m(\theta)$	$J_t(\theta)$	$\ \widehat{u}\ $	$\ \bar{u}\ $	$\widehat{T}$	$\bar{T}$
Design 2a	350.86	1855.4	3.5224	53.560	0.9981	2.109
Design 2A	164.04	1753.6	2.2592	12.1389	0.9049	2.1697
Design 2b	347.32	1874.7	3.8300	52.242	1.0457	2.7952
Design 2B	156.20	1886.1	3.0133	15.246	0.9923	2.1489
Design 2c	814.94	1874.7	127.36	416.61	1.0457	2.7952
Design 2C	327.53	2032.2	55.0129	192.24	1.0517	2.1649
Design 2d	551.70	963.79	126.97	394.31	0.5236	1.8108
Design 2D	152.30	1058.7	32.516	111.15	0.5128	1.3163

while the overall heat transfer performance is maintained. The final design shows complex lattice structures that can be created with current additive manufacturing technologies.

Finally, limitations of this method and future work are addressed. First, the proposed method uses a design-dependent heat source to replace an accurate fluid mechanics model. It does not contain a velocity field and therefore it could not reflect the temperature gradient caused by forced convection in the fluid. Consequently the method is limited to the investigation of problems where the velocity difference in the fluid is small. Secondly, the results of numerical example show that the method does not

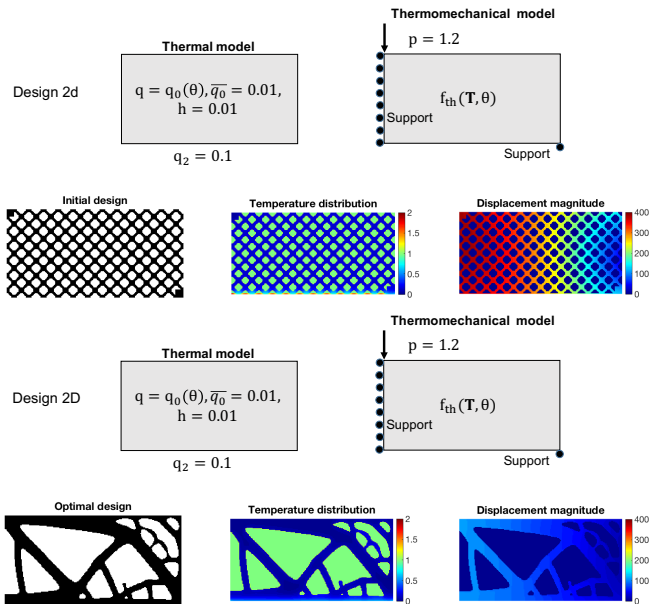


**FIGURE 10.** TOPOLOGY, TEMPERATURE DISTRIBUTION, AND DISPLACEMENT MAGNITUDE DISTRIBUTION OF INITIAL AND OPTIMAL DESIGN FOR SCENARIO 2d AND 2D.

always maintain the local heat transfer performance. For a detailed design, thermal-fluid-structure coupled simulation and experimental study is also required.

## REFERENCES

- [1] Feng, S., Kuang, J., Wen, T., Lu, T., and Ichimiya, K., 2014. "An experimental and numerical study of finned metal foam heat sinks under impinging air jet cooling". *International Journal of Heat and Mass Transfer*, **77**, pp. 1063–1074.
- [2] Al-Athel, K. S., Aly, S. P., Arif, A. F. M., and Mostaghimi, J., 2017. "3d modeling and analysis of the thermo-mechanical behavior of metal foam heat sinks". *International Journal of Thermal Sciences*, **116**, pp. 199–213.
- [3] Paknezhad, M., Rashidi, A., Yousefi, T., and Saghir, Z., 2017. "Effect of aluminum-foam heat sink on inclined hot surface temperature in the case of free convection heat transfer". *Case studies in thermal engineering*, **10**, pp. 199–206.
- [4] Murr, L. E., Gaytan, S. M., Ramirez, D. A., Martinez, E., Hernandez, J., Amato, K. N., Shindo, P. W., Medina, F. R., and Wicker, R. B., 2012. "Metal fabrication by additive manufacturing using laser and electron beam melting technologies". *Journal of Materials Science & Technology*, **28**(1), pp. 1–14.
- [5] Hussein, A., Hao, L., Yan, C., Everson, R., and Young, P., 2013. "Advanced lattice support structures for metal additive manufacturing". *Journal of Materials Processing Technology*, **213**(7), pp. 1019–1026.
- [6] Beyer, C., and Figueroa, D., 2016. "Design and analysis of lattice structures for additive manufacturing". *Journal of Manufacturing Science and Engineering*, **138**(12), p. 121014.
- [7] Queheillalt, D. T., Carbajal, G., Peterson, G., and Wadley, H. N., 2008. "A multifunctional heat pipe sandwich panel structure". *International Journal of Heat and Mass Transfer*, **51**(1-2), pp. 312–326.
- [8] Son, K. N., Weibel, J. A., Kumaresan, V., and Garimella, S. V., 2017. "Design of multifunctional lattice-frame materials for compact heat exchangers". *International Journal of Heat and Mass Transfer*, **115**, pp. 619–629.
- [9] Bunker, R. S., 2004. "Latticework (vortex) cooling effectiveness: Part I stationary channel experiments". In *ASME Turbo Expo 2004: Power for Land, Sea, and Air*, American Society of Mechanical Engineers, pp. 909–918.
- [10] Acharya, S., Zhou, F., Lagrone, J., Mahmood, G., and Bunker, R. S., 2005. "Latticework (vortex) cooling effectiveness: Rotating channel experiments". *Journal of turbomachinery*, **127**(3), pp. 471–478.
- [11] Rao, Y., and Zang, S., 2014. "Flow and heat transfer characteristics in latticework cooling channels with dimple vortex generators". *Journal of Turbomachinery*, **136**(2), p. 021017.
- [12] Au, K., and Yu, K., 2007. "A scaffolding architecture for conformal cooling design in rapid plastic injection moulding". *The International Journal of Advanced Manufacturing Technology*, **34**(5-6), pp. 496–515.
- [13] Au, K., and Yu, K., 2011. "Modeling of multi-connected porous passageway for mould cooling". *Computer-Aided Design*, **43**(8), pp. 989–1000.
- [14] Brooks, H., and Brigden, K., 2016. "Design of conformal cooling layers with self-supporting lattices for additively manufactured tooling". *Additive Manufacturing*, **11**, pp. 16–22.
- [15] Sigmund, O., 2001. "Design of multiphysics actuators using topology optimization—part i: One-material structures". *Computer methods in applied mechanics and engineering*, **190**(49), pp. 6577–6604.
- [16] Sigmund, O., 2001. "Design of multiphysics actuators using topology optimization—part ii: Two-material structures". *Computer methods in applied mechanics and engineering*, **190**(49-50), pp. 6605–6627.
- [17] Du, Y., Luo, Z., Tian, Q., and Chen, L., 2009. "Topology optimization for thermo-mechanical compliant actuators using mesh-free methods". *Engineering Optimization*, **41**(8), pp. 753–772.
- [18] Thurier, P. F., 2014. "A two-material topology optimization method for the design of a passive thermal control interface".

- [19] Zhang, W., Yang, J., Xu, Y., and Gao, T., 2014. “Topology optimization of thermoelastic structures: mean compliance minimization or elastic strain energy minimization”. *Structural and Multidisciplinary Optimization*, **49**(3), pp. 417–429.
- [20] Gao, T., Xu, P., and Zhang, W., 2016. “Topology optimization of thermo-elastic structures with multiple materials under mass constraint”. *Computers & Structures*, **173**, pp. 150–160.
- [21] Wu, T., Liu, K., and Tovar, A., 2017. “Multiphase topology optimization of lattice injection molds”. *Computers & Structures*, **192**, pp. 71–82.
- [22] Wu, T., and Tovar, A., 2018. “Multiscale, thermomechanical topology optimization of self-supporting cellular structures for porous injection molds”. *Rapid Prototyping Journal*.
- [23] Alexandersen, J., Aage, N., Andreasen, C. S., and Sigmund, O., 2014. “Topology optimisation for natural convection problems”. *International Journal for Numerical Methods in Fluids*, **76**(10), pp. 699–721.
- [24] Sato, Y., Yaji, K., Izui, K., Yamada, T., and Nishiwaki, S., 2017. “An optimum design method for a thermal-fluid device incorporating multiobjective topology optimization with an adaptive weighting scheme”. *Journal of Mechanical Design*.
- [25] Zhao, X., Zhou, M., Sigmund, O., and Andreasen, C., 2018. “A poor man’s approach to topology optimization of cooling channels based on a darcy flow model”. *International Journal of Heat and Mass Transfer*, **116**, pp. 1108–1123.
- [26] Gao, T., Zhang, W., Zhu, J., Xu, Y., and Bassir, D., 2008. “Topology optimization of heat conduction problem involving design-dependent heat load effect”. *Finite Elements in Analysis and Design*, **44**(14), pp. 805–813.
- [27] Iga, A., Nishiwaki, S., Izui, K., and Yoshimura, M., 2009. “Topology optimization for thermal conductors considering design-dependent effects, including heat conduction and convection”. *International Journal of Heat and Mass Transfer*, **52**(11), pp. 2721–2732.
- [28] Dede, E. M., Nomura, T., and Lee, J., 2014. *Multiphysics Simulation*. Springer.
- [29] Joo, Y., Lee, I., and Kim, S. J., 2017. “Topology optimization of heat sinks in natural convection considering the effect of shape-dependent heat transfer coefficient”. *International Journal of Heat and Mass Transfer*, **109**, pp. 123–133.